Experimental Analysis of Rotor-Stator Contact with Many Degrees of Freedom

Oliver Alber

Abstract The dynamics of a multi disk rotor contacting a non-rotating stator with many degrees of freedom is analyzed experimentally. For this task a test rig is built up and described in the paper. Experimental results for slow run-ups and run-downs as well as orbits and frequency spectra are presented showing synchronous motion as well as backward whirl motion. The results validate the applicability of models with many degrees of freedom for rotor and for stator. A forced modal decoupling method is applied to the MDOF system and demonstrates that in a limited rotation speed regime simple SDOF models for rotor-stator contact are able to sufficiently describe the experimentally observed dynamics.

Keywords Rotor-stator contact · Rub · Modal decoupling · MDOF · Experimental

1 Introduction

The dynamics during contact of a JEFFCOTT rotor with a flexibly mounted rigid stator has been subject of various previous literature (e.g. [1, 2]), a comprehensive overview of current research is given in [3]. At least the synchronous motion during contact of rotor and stator, its stability and the backward whirl motion can be described quite accurately. Many parameter studies revealed the influence of critical system parameters as well as the conditions for the onset and stability of different motion patterns for this nonlinear problem. In contrast to this simple system, in technical applications the rotor as well as the stator structure (e.g. housing or backup bearing) always exhibit infinite resonance frequencies. Therefore the investigation of systems with many degrees of freedom (MDOF) is very promising,

O. Alber (✉)
TU Darmstadt, Institute for Structural Dynamics, Otto-Berndt-Str, 2,
64287 Darmstadt, Germany
e-mail: alber@sdy.tu-darmstadt.de

P. Pennacchi (ed.), *Proceedings of the 9th IFToMM International Conference on Rotor Dynamics*, Mechanisms and Machine Science 21,
DOI 10.1007/978-3-319-06590-8_160

as the dynamics of almost all technical systems can be sufficiently described by a finite amount of DOF, e.g. by using GALERKIN's method, Finite Element Method or system reduction techniques like GUYAN or CRAIG-BAMPTON method. MDOF rotors are used e.g. in [4, 5]. In addition MDOF stators are taken into account by Wegener [6]. However, for rotor-stator contact it is not clear how interacting modes influence the system dynamics. An analytical solution for the synchronous motion of MDOF systems during Rotor-Stator contact was derived by Wegener [7] and applied by Alber [8]. In [8] also a stability analysis for this particular motion is applied, which is already well-known for the simple system [7]. Results point out that these analytical predictions fit well to numerical simulation results of the non-linear MDOF system. Experimental validation is still pending and scope of this work. If only one mode of each rotor and stator are dominating the motion of the system the MDOF system can even be reduced to the simple single degree of freedom (SDOF) system mentioned above by applying a forced modal decoupling method [9]. If a modal reduction is not possible, for systems with many degrees of freedom also additional effects arise, for example the coexistence of several backward whirl motions [10, 11]. These motions usually cause high vibration amplitudes of rotor and stator as well as high contact forces and can be very dangerous to the system. These assumptions are proved by experimental results in the presented paper.

2 Test Rig Assembly and Properties

The test rig presented in Fig. 1 utilizes a building kit of the Institute for Structural Dynamics analogously to [2, 7, 12], which is optimized for studying fundamental rotordynamic effects in small-scale, e.g. fluid film bearings, AMBs, vibration reduction with ERFs or systems with significant gyroscopic influence. Figures 1 and 2 show all elements of the test rig. This includes the shaft (d) made of high-strength steel, which is mounted with three ball bearings in very stiff bearing supports (b), one bearing at the left and two bearings at the right side of the disks. Two rigid disks (c) are fixed on the shaft using a conical clamping mechanism, which ensures an almost rigid connection between the disks and the shaft. Unbalance masses can be added to the disks. At the left disk a mounting for the contact ring of the rotor (m) is provided. Contact rings of different sizes and materials or contact rings with roller bearings can be used, hereby the friction coefficient or the gap size between rotor and stator contact surfaces can be varied. The position of the two disks in the *yz* plane is measured by non-contacting eddy current displacement sensors [ECDS, (g)]. The angular velocity of the shaft is measured by an incremental encoder (a). A speed-regulated direct current motor (f) is driving the rotor using a flexible Double Loop Coupling (e). At location D a viscous oil damper (Fig. 1 bottom) can be added to the rotor in addition. The mass of the oil damper bearing is small compared to the mass of the two disks and therefore neglected.

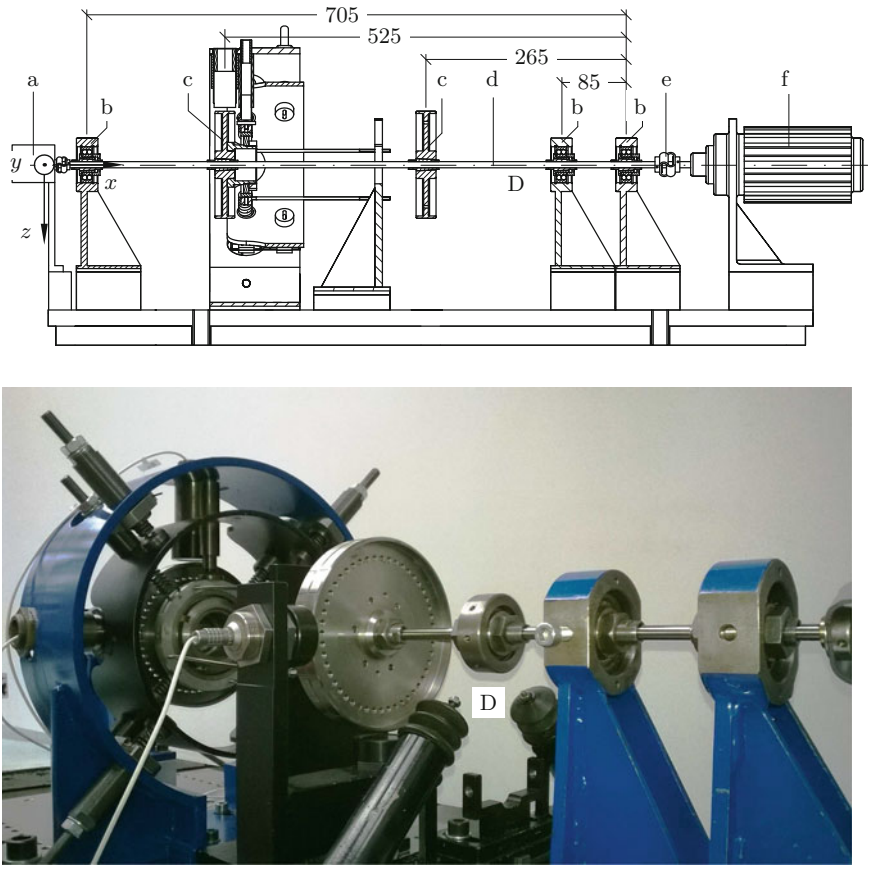

Fig. 1 Assembly of the test rig for the experimental analysis of rotor-stator contact with many degrees of freedom (all lengths in mm)

The stator consists of an inner aluminum ring (h) with a steel contact surface (l), which is mounted on an outer stator ring (n) with four elastic springs (i). The outer stator ring is mounted at the stator cage with four additional springs. The lower spring housings can be filled with oil in order to adjust the stator damping. The position in the *yz* plane of the inner stator ring is measured with two small ECDS (k). Rotation of the stator around the *x*-, *y*- or *z*-axis is avoided by guiding the stator rings with four beams each [(j) and (o), details in Fig. 3]. All lengths of the rotor are provided in Fig. 1, system parameters can be found in Table 1. In order to calculate the mass matrix of the rotor M_R, the mass of the shaft between the two left bearings is added to the mass of the two disks. Resonance frequencies, modeshapes, and damping coefficients of rotor and stator are measured by experimental modal analysis (EMA) with and without the viscous damper. Rotor resonance frequencies are compared to the results of the FEM model of a continuous shaft with two rigid

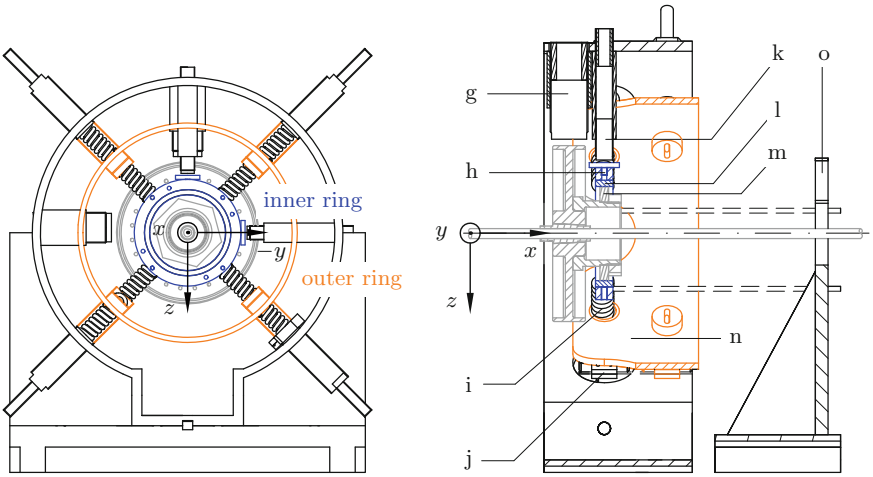

Fig. 2 Assembly of the stator system with moving inner and outer ring (2 DOF)

mass disks. The symmetric stiffness matrices K_R and K_S of rotor and stator are derived using the measured resonance frequencies ω_i, modeshapes $\widehat{\boldsymbol{q}}_i$ and mass matrices of the rotor and stator M according to

$$\boldsymbol{Q}^T\boldsymbol{K}\boldsymbol{Q} = \begin{bmatrix} \widehat{\boldsymbol{q}}_1^T \\ \widehat{\boldsymbol{q}}_2^T \end{bmatrix} \begin{bmatrix} k_{11} & k_{12} \\ k_{12} & k_{22} \end{bmatrix} [\, \widehat{\boldsymbol{q}}_1 \quad \widehat{\boldsymbol{q}}_2 \,] = \begin{bmatrix} \widehat{\boldsymbol{q}}_1^T \boldsymbol{M} \widehat{\boldsymbol{q}}_1 \omega_1^2 & 0 \\ 0 & \widehat{\boldsymbol{q}}_2^T \boldsymbol{M} \widehat{\boldsymbol{q}}_2 \omega_2^2 \end{bmatrix}. \quad (1)$$

It is possible to change springs or add additional weight to the inner ring of the stator in order to change the resonance frequency of the stator. The prestress of the springs is adjustable in order to center the rotor in the stator or introduce a static offset between rotor and stator.

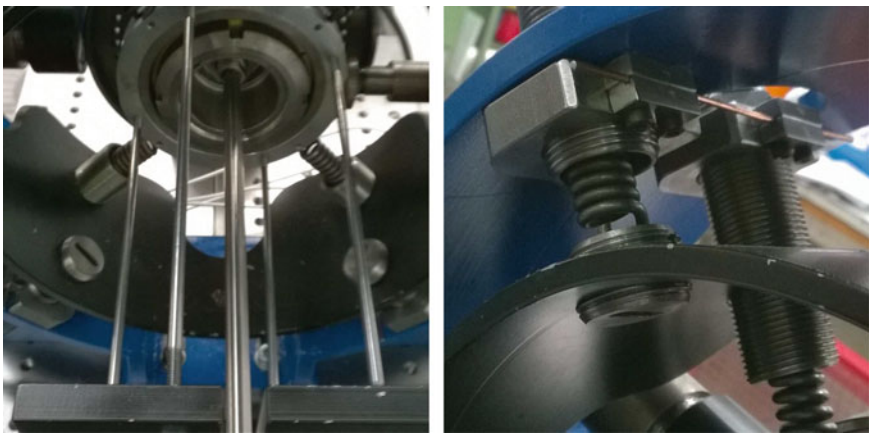

Fig. 3 Guiding beams for the inner (o, *left*) and outer (j, *right*) stator ring

Table 1 Parameters used in the test rig

Parameter	Symbol	Unit	Value	Source
Shaft diameter	d_R	mm	8	Measurement
Young's modulus of shaft	E	N/mm^2	2.1×10^5	Literature
Mass of left disk	m_1	kg	1.35	Measurement
Mass of right disk	m_2	kg	1.04	Measurement
Mass matrix of rotor	M_R	kg	$\begin{bmatrix} 1.41 & 0 \\ 0 & 1.10 \end{bmatrix}$	Calculation
Stiffness matrix of rotor	K_R	N/m	$\begin{bmatrix} 52986 & -46015 \\ -46015 & 71220 \end{bmatrix}$	Calculation
1st resonance frequency	$\omega_{R1}/2\pi$	Hz	17.3	Measurement (EMA)
(U shape bending mode)		Hz	17.7	Calculation (FEM)
Damping ratio	D_{R1}	%	0.14	Measurement
Damping ratio with damper	D_{R1d}	%	5.1	Measurement
2nd resonance frequency	$\omega_{R2}/2\pi$	Hz	47.6	Measurement (EMA)
(S shape bending mode)		Hz	46.1	Calculation (FEM)
Damping ratio	D_{R2}	%	0.8	Measurement
Damping ratio with damper	D_{R2d}	%	1.9	Measurement
3rd resonance frequency	$\omega_{R3}/2\pi$	Hz	130.8	Measurement (EMA)
Mass of inner stator ring	m_{S1}	kg	0.3	Measurement
Mass of outer stator ring	m_{S2}	kg	2.8	Measurement
Stiffness matrix of stator	K_S	N/m	$\begin{bmatrix} 97700 & -61840 \\ -61840 & 192240 \end{bmatrix}$	Calculation
1st resonance frequency	$\omega_{S1}/2\pi$	Hz	36.5	Measurement (EMA)
Damping ratio	D_{S1}	%	1.4	Measurement (EMA)
2nd resonance frequency	$\omega_{S2}/2\pi$	Hz	92.9	Measurement (EMA)
Damping ratio	D_{S2}	%	0.5	Measurement (EMA)
1st cage res. frequency	$\omega/2\pi$	Hz	245	Measurement (EMA)
Friction coeff. (brass/steel)	μ_F	1	0.15	Parameter fitting
Average nominal gap	s	mm	0.5	Measurement

The signal processing is similar to [2]. The synchronous motor (f) is controlled by a ramp generator, which allows a linear increase or decrease of the rotation speed Ω. The signal of the incremental encoder (a) is amplified and transformed into sine and cosine signals in order to determine rotation angle $\varphi(t)$ and rotation speed $\dot{\varphi}(t)$ by software after sampling. For signal processing of the rotor and stator ECDS (g, k) signals, analog signal conditioning cards are used, which compensate the influence of temperature and amplify the signal. Data acquisition of all analog signals is performed using a signal acquisition card with anti-aliasing filter and simultaneous sample and hold. The position signals of the two rotor disks and the inner stator ring are corrected from the static offset value and the runout error by using the signal of a quasi-static run with a very low rotation speed. Vertical and horizontal position signals are transformed into complex signals.

3 Rotor-Stator Contact of MDOF Systems

The model for Rotor-Stator Contact of MDOF systems shown in Fig. 4 is presented in [7, 8]. It consists of an isotropic multi disk rotor with mass matrix $\boldsymbol{M}_R$, symmetric stiffness matrix $\boldsymbol{K}_R$ and mass excentricity ε_M, which may contact an isotropic system of flexibly mounted rigid stator rings with mass matrix $\boldsymbol{M}_S$ and stiffness matrix $\boldsymbol{K}_S$. Both rotor and stator account for modal damping with damping ratios D_{Si} and D_{Ri}. The contact areas of rotor and stator are cylindrical surfaces with an average clearance s and dry friction coefficient μ_F. The positions of the contacting degrees of freedom $r_{RC} = \boldsymbol{l}_R^T r_R$ and $r_{SC} = \boldsymbol{l}_S^T r_S$ are described by the position vectors $\boldsymbol{l}_R$ and $\boldsymbol{l}_S$, which contain elements with values of unity for the contact position and otherwise zero. The contact force F_C used for numerical simulation is described by

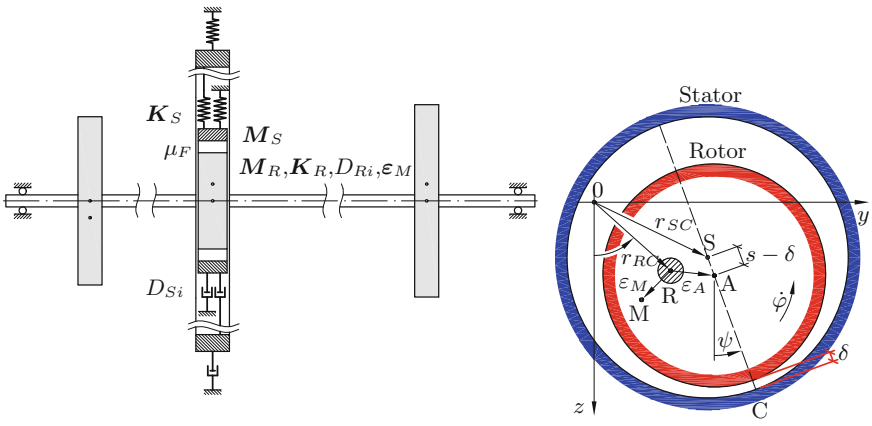

Fig. 4 MDOF model and contact kinematics (from [2]) for rotor-stator contact

a pseudo-linear viscoelastic contact element (contact stiffness k_C, contact damping b_C) according to [2]:

$$F_C = (1 + i\mu_F)\left\langle -k_C\delta - b_C\left\langle \dot{\delta}\right\rangle\right\rangle\langle -\delta\rangle^0 e^{i\psi} \tag{2}$$

with $\langle x\rangle = x$ for $x > 0$. The minimal gap between rotor and stator δ and the contact force normal direction ψ can be derived by using

$$r_{RC} + \varepsilon_A e^{i\varphi} - r_{SC} = (s - \delta)e^{i\psi}. \tag{3}$$

The equations of motion for rotor and stator displacements r_R and r_S are

$$\boldsymbol{M}_R\ddot{\boldsymbol{r}}_R + B_R\dot{\boldsymbol{r}}_R + K_R\boldsymbol{r}_R = -\boldsymbol{M}_R\varepsilon_M(e^{i\varphi})^{\cdot\cdot} - \boldsymbol{l}_R F_C, \tag{4}$$

$$\boldsymbol{M}_S\ddot{\boldsymbol{r}}_S + B_S\dot{\boldsymbol{r}}_S + K_S\boldsymbol{r}_S = \boldsymbol{l}_S F_C\,. \tag{5}$$

For this system with many degrees of freedoms and a single contact position an analytical approximation for the stationary synchronous motion (constant Ω) is described in [7] and stability analysis is presented in [8].

The dynamics of the model is compared to experimental results in Fig. 5. Therefore slow run-ups and run-downs (3370 rpm passed in 102 s) as well as orbits and spectra are presented. The mass excentricities are $|\varepsilon_{M1}|e^{i\,\varphi_{M1}}$ for the left mass disk and $|\varepsilon_{M2}|e^{i\,\varphi_{M2}}$ for the right mass disk. The numerical simulation by direct time integration (ODE15 s in MATLAB) of the nonlinear equations on the right side of

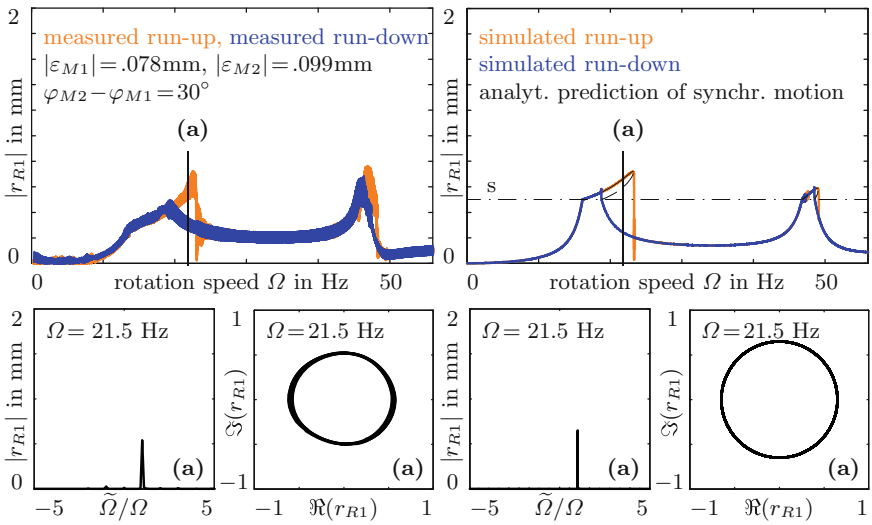

Fig. 5 Rotor deflection amplitude $|r_{R1}|$ of contacting disk with viscous damper, measured (*left*) and simulated (*right*), as well as spectra and orbits

Fig. 5 shows qualitatively good agreement with the experimental results on the left side. Also the analytical solution for the synchronous motion (black) from [7] as well as the stability analysis for this motion (solid: stable, dashed: unstable) from [8] predicts the measured motion well. In the first resonance a synchronous motion with contact is established, orbits and spectra are presented. After the first resonance the rotor separates from the stator and contacts again in the second resonance. The measured signal shows small bearing anisotropy. Contact establishes at subtly different rotor deflection amplitudes for different resonances.

The occurrence of a second rotor resonance might also trigger a particular backward whirl motion. Figure 6 shows the measured runup and rundown for the system without the viscous damper. Reduced damping leads to an increased danger of backward whirl motion [1, 2, 13]. During the run-down the rotor does not separate from the stator between the first and second rotor resonance. A backward whirl motion is observed in the orbit and spectrum, in these figures the simulated result (gray) matches the measurement (blue). The Short Time Fast Fourier Transform (STFFT) of the run-down time signal indicates in addition to the synchronous frequency component a negative frequency component with $\psi \approx -18$ Hz in a large rotation speed regime, which is slightly larger than the first rotor resonance frequency ($\omega_{R1}/2\pi = 17.3$ Hz) but significantly smaller than the first resonance frequency of the rigidly coupled rotor-stator system ($s = 0$ leads to $\omega_{RS1}/2\pi = 29.1$ Hz). Backward whirl is observed in the whole range between both rotor resonances. Other backward whirl motions are not excited in this example. The backward whirl motion can be estimated with an analytical method [10], which delivers a good prediction for the occurring rotor deflection (solid black line in the run-down).

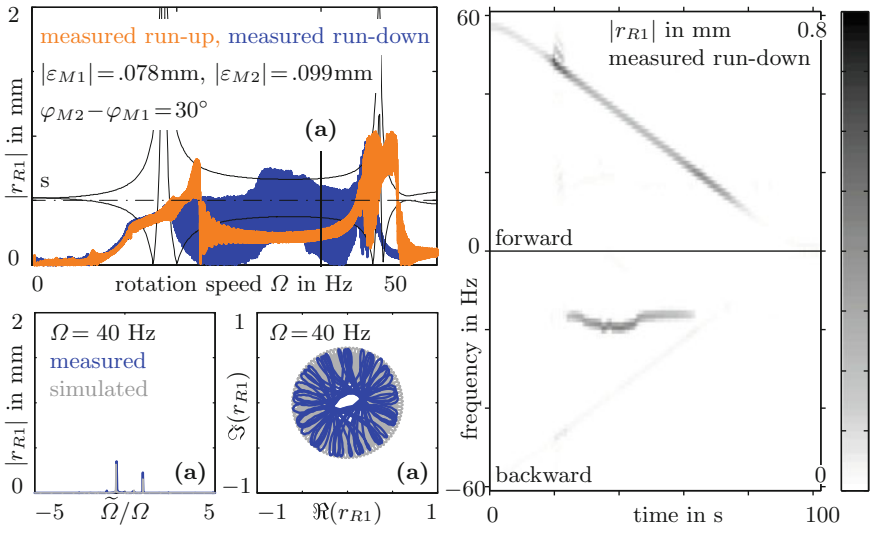

Fig. 6 Measured rotor deflection amplitude $|r_{R1}|$ of contacting disk without viscous damper as well as spectra, orbits and STFFT of measured run-down

4 Applicability of Forced Modal Decoupling

At least in particular regimes it is possible to reduce the MDOF system to a JEFFCOTT rotor contacting a SDOF stator, e.g. from [2], by applying a forced modal decoupling method. In [9] a transformation to the modal coordinates $\boldsymbol{p}(t)$ of the uncoupled rotor and stator

$$\boldsymbol{r}_R(t) = \boldsymbol{Q}_R \boldsymbol{p}_R(t), \quad \boldsymbol{r}_S(t) = \boldsymbol{Q}_S \boldsymbol{p}_S(t), \tag{6}$$

using the modal matrices $\boldsymbol{Q}_R$ and $\boldsymbol{Q}_S$ is performed. Taking into account only the n-th rotor mode and the m-th stator mode, normalizing the contacting coordinates of these modes to one ($\widehat{q}_{RnC} = \widehat{q}_{SmC} = 1$) and neglecting all other modes, one obtains the reduced equations

$$m_{Rn}\ddot{\widetilde{r}}_R(t) + b_{Rn}\dot{\widetilde{r}}_R(t) + k_{Rn}\widetilde{r}_R(t) = -(\boldsymbol{Q}_R^T \boldsymbol{M}_R \varepsilon_M)_n (e^{i\varphi})^{\cdot\cdot} - \tilde{F}_C(t), \tag{7}$$

$$m_{Sm}\ddot{\widetilde{r}}_S(t) + b_{Sm}\dot{\widetilde{r}}_S(t) + k_{Sm}\widetilde{r}_S(t) = \tilde{F}_C(t), \tag{8}$$

$$\widetilde{r}_R(t) + \varepsilon_A e^{i\varphi} - \widetilde{r}_S(t) = s\,\frac{1 - i\mu_F}{\sqrt{1+\mu_F^2}}\,\frac{\tilde{F}_C(t)}{|\tilde{F}_C(t)|} \tag{9}$$

with the modal parameters of the n-th rotor mode $\langle\rangle_{Rn}$ and the m-th stator mode $\langle\rangle_{Sm}$. $\langle\rangle_n$ and $\langle\rangle_m$ are the n-th and m-th matrix rows and $\widetilde{\langle\rangle}$ are the approximated state variables. Equation (9) is a kinematic contact condition, which can be used for continuous contact of rotor and stator instead of Eq. (2). This form does exactly match to the simple rotor-stator contact system analyzed for example by Black and Ehehalt [1, 2]. The results of the reduced model (Fig. 7) can be compared to the measured dynamics for rotor-stator contact of the MDOF system of Fig. 5. On the left side of Fig. 7 the modal content of a simulated run-up is displayed. In the first rotor resonance the first rotor mode and the second stator mode are dominant. The stator modes only contribute to a small extent to the overall motion. Considering

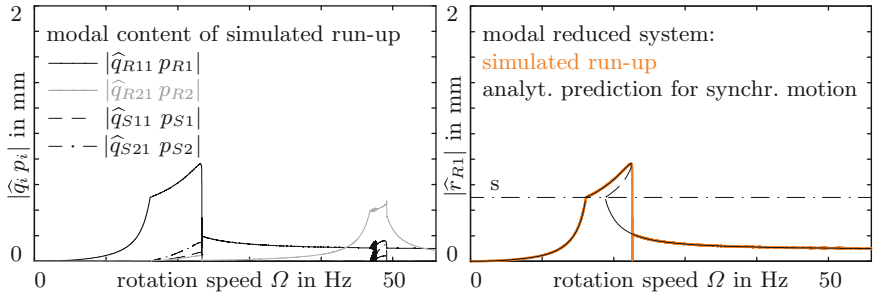

Fig. 7 Modal content of MDOF system (simulated run-up) and modal reduced system only considering 1st rotor and 2nd stator mode

only the first rotor and the second stator mode, the measured system dynamics in the first resonance can be described quite well by the modal reduced system, which is presented on the right side of Fig. 7. Results are not valid around the second rotor resonance frequency.

5 Conclusions

The presented test rig is utilized to experimentally demonstrate the dynamics of rotor-stator contact systems with many degrees of freedom. For the provided parameters synchronous motion as well as backward whirl motion are observed. It is shown that the measured dynamics can be modeled with a non-linear MDOF rotor-stator contact model described in the paper. Previous analytical predictions for the synchronous motion and its stability as well as for the backward whirl motion show good agreement to the experimentally observed behaviour. Backward whirl motion is obtained for low damping in a wide frequency range and triggered while passing the second resonance during run-down. The method of forced modal decoupling is successfully applied to predict the dynamics of the MDOF system in a limited regime using the well-known simple SDOF model for rotor-stator contact.

References

1. Black HF (1968) Interaction of a whirling rotor with a vibrating stator across a clearance annulus. J Mech Eng Sci 10:1–12
2. Ehehalt U (2008) Bewegungsformen elastischer Rotoren bei Statorkontakt. Fortschr.-Ber. VDI Reihe 11 Nr. 335. VDI Verlag, Düsseldorf
3. Jacquet-Richardet G et al (2013) Rotor to stator contacts in turbomachines. Review and application. Mech Syst Signal Process 40:401–420
4. Pennacchi P, Bachschmid N, Tanzi E (2013) Light and short arc rubs in rotating machines: experimental tests and modelling. Mech Syst Signal Process 23:2205–2227
5. Isaksson JL (1996) Unbalance response analysis of a two-mass rotor system including rubbing effects. IMechE 6:395–403
6. Cole MOT (2008) On stability of rotordynamic systems with rotor-stator contact interaction. Proc R Soc A 464:3353–3375
7. Wegener G (2000) Elastische Fanglager zur Amplitudenbegrenzung elastischer Rotoren. Fortschr.-Ber. VDI Reihe 11 Nr. 290. VDI Verlag, Düsseldorf
8. Alber O (2012) Rotor stator interaction with many degrees of freedom. Proc Appl Math Mech 12(1):251–252
9. Alber O, Markert R (2013) Modale Zwangsentkopplung bei Rotor-Stator-Kontakt mit mehreren Freiheitsgraden. In: 10th SIRM, Berlin, pp 1–10
10. Alber O, Norrick N, Siegl B (2013) Multimode backward whirl motion in rotor-stator contact. In: 11th ICOVP, Lisbon, pp 1–10
11. Childs DW, Bhattacharya A (2007) Prediction of dry-friction whirl and whip between a rotor and a stator. J Vib Acoust 129:355–362
12. Wieland G (2014) Fanglager mit veränderbaren Parametern. TU-Prints, Darmstadt
13. Bartha AR (2000) Dry friction backward whirl of rotors. Ph.D. thesis, ETH Zürich